Nasal Similarity Measure of 3D Faces Based on Curve Shape Space

Article *in* Pattern Recognition · December 2018

DOI: 10.1016/j.patcog.2018.12.006

CITATION
1

READS
75

5 authors, including:

Lv Chenlei
Nanyang Technological University
14 PUBLICATIONS **8** CITATIONS
SEE PROFILE

zk wu
Beijing Normal University
162 PUBLICATIONS **732** CITATIONS
SEE PROFILE

Xingce Wang
Beijing Normal University
58 PUBLICATIONS **199** CITATIONS
SEE PROFILE

Mingquan Zhou
Beijing Normal University
219 PUBLICATIONS **955** CITATIONS
SEE PROFILE

Pattern Recognition 88 (2019) 458–469

Contents lists available at ScienceDirect

Pattern Recognition

journal homepage: www.elsevier.com/locate/patcog

Nasal similarity measure of 3D faces based on curve shape space

Chenlei Lv[a,c], Zhongke Wu[a,c,*], Xingce Wang[a,c], Mingquan Zhou[a,c], Kar-Ann Toh[b]

[a] Engineering Research Center of Virtual Reality and Applications, Ministry of Education, Beijing Key Laboratory of Digital Preservation and Virtual Reality for Cultural Heritage, Beijing Normal University, Beijing, 100875, China
[b] School of Electrical and Electronic Engineering, Yonsei University, Seoul, South Korea
[c] College of Information Science and Technology, Beijing Normal University, Beijing, China

ARTICLE INFO

Article history:
Received 12 March 2018
Revised 9 November 2018
Accepted 8 December 2018
Available online 8 December 2018

Keywords:
Shape space
Nose similarity measure
Riemannian manifold

ABSTRACT

We propose a novel method for measuring the nasal similarity among 3D faces. Firstly, we construct a representation for the nose shape, which is composed of a set of geodesic curves, each crosses the bridge of the nose. Next, using these geodesic curves, we formulate a similarity measure to compare among noses in the curve shape space. Under the Riemannian framework, the shape space is a quotient space for which the scaling, translation and rotation are removed. Since the nose similarity measure is based on the shape comparison, the proposed method has the following advantages: (1) the similarity measure is robust to facial expressions since the nose is not affected by facial expressions; (2) the geometric features of the nose shape match well with the human perception; (3) the similarity measure is independent of the mesh grid because the chosen nose curves are not sensitive to the triangular mesh model. We construct a nasal hierarchical structure for noses organization which is based on nose similarity measure results. In our experiments, we evaluate the performance of the proposed method and compare it with competing methods on three public face databases namely, FRGC2.0, Texas3D and BosphorusDB. The results show superiority of the proposed method in terms of both the speed and the accuracy when the nasal measurements are processed in the nasal hierarchical structure and the nasal samples with low sampling rate (5%-25% of original point cloud).

1. Introduction

Human biometric information analysis is a popular field which involves machine learning, computer vision and computer graphics. There are many applications that utilize biometric information such as criminal investigation, cosmetic surgery and social security. However, a global analysis of the human face poses challenges such complex pre-processing, varying facial expressions and different qualities of facial data. Instead of the global facial data analysis, using partial data, especially the nose, is a feasible solution to deal with these challenges ([1,2]).

Previous research on nose analysis focused on nasal feature extraction [3] and recognition [4]. A quantitative analysis of the nose information has not been studied seriously such as nasal similarity measure. The similarity measures of noses is the fundamental component of nose clustering. In 2D face images, the nasal feature analysis is limited by illumination, head poses and image noise. Ever since the remarkable development of 3D scanning equipment over the years, capturing high resolution 3D scanning data becomes viable. The nose in 3D facial data has complete geometrical information. The nose region on the facial surface has relatively low distortion, such as holes, self-intersections and obvious refraction angles. Therefore, our similarity measure framework is focused on the nose in 3D facial data.

Our nasal similarity measure framework is based on the shape space theory. Firstly, we construct nose curves from the nose on a 3D facial surface. Secondly, we embed the curves into the shape space of Riemannian manifold. Finally, we propose a metric for the shape space to compare the similarity between noses. We assign different weights to nose curves to measure the results and combine them to achieve the nasal similarity measure. Using the measure of the nose, we propose the concept of a mean nose and establish a hierarchical structure of noses to provide additional guidance information in the framework. In summary, our main contributions are as follows:

1) We present a representation of the nose shape, which is constructed from a set of registered nose curves.
2) We propose a nasal similarity measure based on the metric of nose curves in the shape space.

* Corresponding author.
E-mail addresses: chenleilv@mail.bnu.edu.cn (C. Lv), zwu@bnu.edu.cn (Z. Wu), wangxingce@bnu.edu.cn (X. Wang), mqzhou@bnu.edu.cn (M. Zhou), katoh@yonsei.ac.kr (K.-A. Toh).

https://doi.org/10.1016/j.patcog.2018.12.006
0031-3203/

3) We propose the concept of mean nasal shape and construct a hierarchical structure of noses as a tool for statistical analysis.

The remaining parts of the paper are organized as follows. In Section 2, we present some related works on biological characteristics analysis. In Section 3, we illustrate the basic knowledge of the shape space for immediate reference. We show the details of the nose measure in Section 4, and dummyTXdummy- we provide applications and experiments on public facial databases in Section 5.

Abbreviations:

$d(N_1, N_2)$: The similarity measure between two nose shapes N_1 and N_2; N_c: nose shape; C_n: nose curve; $G(c, l)$: geodesic path in surface from point c to l; cn: point in geodesic circle; ln: point in nose bridge curve; C_v: arc length parametrization of the nose curve; C_{vs}: nose curve which remove the scaling influence; C_{vs}': nose curve which aligned by local coordinate system; $G_s(C_1, C_2)$: nose curves measurement in shape space;

2. Related works

The nasal similarity measure can be traced to facial similarity measure. For facial similarity measure, previous studies focused on 2D facial image feature extraction and comparisons. Tredoux [5] defined a distance between two faces in the mathematical space based on principal component analysis. Chopra [6] used convolutional networks to map the images to a low-dimensional space.Schroff [7] proposed a data-driven method that is based on the pixel structure in face images. Some works were focus on the part facial features analysis. Mostafa [8] proposed a facial tracking method based on particle filter in regions of interest (ROI). The author also proposed a facial landmarks detection method [9] based on part-based model. Barkouky [10] proposed a method based on selective part model to detect facial features with partial occlusion. Soldera [11] proposed a geodesic distance approximation method to represent the color intensities in the vicinities. As these 2D imaging approaches are highly sensitive to head poses, facial expressions, lighting conditions and natural noise, the geometric features of nose can be extremely difficult to extract. Therefore, adoption of similarity measure based on the facial geometry can be more appropriate for 3D data.

The similarity measure for 3D facial data includes those based on the global 3D face and those based on the local 3D nose geometric features. Those early methods defined the distance between two 3D objects in the R3 space directly. Wang [12] used a partial ICP method to measure the effect of facial expressions. Chang [13] proposed a local region-based method for face recognition. Gokberk [14] proposed a 3D shape analysis technique for face recognition. Mian [15] propose a face recognition algorithm based on multi-modal facial data. Queirolo [16] proposed a 3D face recognition by Simulated Annealing and Surface measure. Some methods are based on the certain facial curves in facial analysis. Li [17] propose a 3D face pose estimation method based on central profile. Efraty [18] also use the facial profile and SVM classification framework in facial recognition. Lei [19] propose a facial signature called Angular Radial Signature (ARS). The features of the ARS are extracted by facial radial curves. The author use Kernel Principal Component Analysis (KPCA) to analysis the features and Support Vector Machine (SVM) to perform face recognition. Mestetskiy [14] proposed a surface measure method to evaluate the quality of 3D face reconstruction. The measure process was based on triangular grids.

In the R^3 space, the representation of 3D data is limited by the coordinate system. Constructing the convenient representation of facial data is necessary which is independent to the coordinate system. Blanz [20] proposed a 3D face synthesis and transformation method called the "Morphable Model". For face recognition, the Morphable Model can achieve valuable results [21]. However, the method is highly dependent on the facial samples available. Moreover, the feature vectors in the face space are counterintuitive to human perception. Lee [22] proposed a 3D deformable model for facial recognition. The method is combining edge, color and wireframe information to build the model. Kakadiaris [23] propose a method with similar idea for facial expressions robust recognition. The author used the framework in face recognition [24] to remove the influence of poses and illuminations. Hu [25] improved the 3D Morphable Model method in 2D image projection process. Walid [26] proposed a 3D face recognition method using covariance based descriptors. Guo [27] proposed an expression invariant 3D face recognition using local shape matching in 3D point cloud with registration. Berretti [28,29] proposed a method which used isogeodesic stripes and 3D weighted walkthroughs for face matching. The relative positions of these stripes are robust to facial expression change. Ahdid [30] extracted the similar geodesic curves to be the representation of facial features.

Some researchers proposed a 3D facial data analysis method based on the Riemannian framework. Bronstein [31,32] proposed a canonical form for 3D faces. Using the geodesic pairs between these discrete points in faces and the multi-dimensional scaling (MDS) to establish the canonical form, the effect of facial expression changes are removed. Xia [33,34] proposed a facial expression invariant method for facial animation geometric compression. Zeng [35,36] applied the Ricci flow for 3D shape analysis. The Ricci flow is a tool for 3D surface curvature analysis, and it is invariant to rigid-body motion and isometric transformation.

Kendall [37] proposed the concept of shape space. The shape space is a Riemannian manifold and quotient space. Anuj [38] followed this basic idea and proposed the square-root velocity (SRV) method. To measure the nose shapes, a search in the geodesic circles on the 3D facial surface is conducted before comparing the circles in the shape space [1]. Amor [39] proposed a Riemannian shape analysis based on the radial curves, with a similar idea. Jermyn [40] extended the curves measure to a surfaces measure problem, and Kurtek [41] used a related result for 3D face analysis. The precision of these methods is also limited by the smoothness of the facial surface.

For partial biometrics matching based on facial data, Yan [42] proposed a 3D ear shape measure method for biometric recognition. Chen [43] constructed a 3D ear matching system with detection, identification and verification modes. Faltemier [44] proposed a method which compares different regions in facial data and combines the final matching results. Chang [45] computed a match score from the regions around the nose for recognition. Emambakhsh [2,46] proposed a 3D nose recognition method by nasal curve matching. Gao [47] proposed 3D Face Recognition based on nasal region. He also used similar idea to improve the accuracy of facial landmarks detection [48]. Zehngut [49] proposed a face recognition method based on nose biometrics information. The nasal features are extracted by Kernel Class-Dependence Feature Analysis. These studies are mostly processed in the Euclidean space which is sensitive to object translation and rotation. Our nasal similarity framework is based on the shape space analysis where robustness to rigid-body changes can be anticipated.

3. Fundamentals

We introduce the theory of shape space and its related methods in this section for immediate reference. The shape space provides a mathematical representation and measure for curves and surface shapes. It also defines some regularities for shape analysis.

In mathematics, the shape space is a theory for describing a group of geometric shapes; it was introduced into the computer science field by Kendall in 1984 [37]. The shape space is a quotient

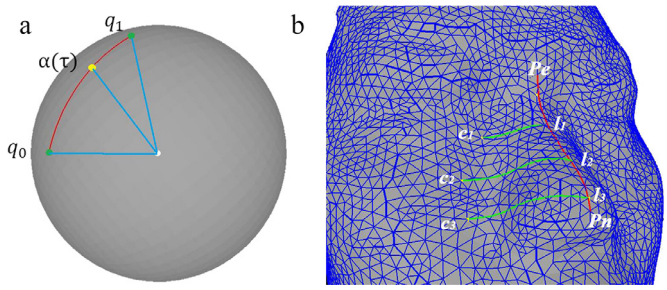

Fig. 1. (a) The shape space and the geodesic path between shapes. (b) Nose curves on a 3D facial surface.

space of isometric Lie group actions. Different similarity transformations, such as scaling, translation and rotation, are regarded as a Lie group that acts smoothly on a manifold. The manifold is constructed by all shape conditions. Defining a metric in a manifold by the geodesic distance, the similarities of different shapes can be computed.

$$M/G = \{[p] | p \in M\} \tag{1}$$

$$d_{M/G}([p],[q]) = \inf_{g \in G} d_M(p, g.q) = \inf_{o \in SO(n)} d_{PM}(p, o.q) \tag{2}$$

In Eq. (1), G is a Lie group that is acting smoothly on a manifold M. For p in M, the orbit of p is defined as $[p]$. The shape space should remove the influence of translation, scaling and rotation. The metric in shape space cannot be achieved easily because the influence of the rotation cannot be removed directly. In general, a pre-shape space is used instead of the strict shape space. The metric in pre-shape space can be achieved which have close relationship with the metric in shape space. Based on the metric in pre-shape space, the metric in shape space can be computed through an indirect method such as procrustes analysis. The pre-shape space is convenient to obtain. In Eq. (2), the metric in shape space is obtained by a group acting process in M. In practice, the metric is computed in the pre-shape space PM. The action group of rotation $SO(n)$ is preserved in the pre-shape space.

For an application of this theory, we introduce the square-root velocity (SRV) [38], which has a close relationship to our method. The SRV is a representation for analysis of shapes and curves. It transfers curves to a certain parameterization and constructs a pre-shape space. In Eq. (3), we show the SRV representation for curves. β is the parameterized curve, and $\|\cdot\|$ is the Euclidean 2-norm that can represent length in general. Here, t is the control parameter, and $t \in (0, 1)$. The pre-shape space is constructed. The rotation of curves is not removed in the pre-shape space. Curves with different rotations are not of the same element in the space. Computing the geodesic distance in pre-shape space should consider the effect of rotation. Procrustes analysis is discussed in [37] to remove the influence of the rotation between two objects.

$$q(t) = \dot{\beta}(t) / \sqrt{\|\dot{\beta}(t)\|} \tag{3}$$

In Eq. (4), q_0 and q_1 are points in the pre-shape space. We achieve the point α in the geodesic path between q_0 and q_1. The point α represents a curve in R^3 space. The curve in R^3 space is represented as a point in shape space. The $\alpha(\tau)$ represents a certain curve in the geodesic path between two curves. θ is the angle of two curves in the shape space where it can represent the distance between the curves. In Eq. (5), we compute the distance between the objects in the shape space. The τ means the index between 0 and 1 in a geodesic path in the shape space. It represents a certain curve in the geodesic path between two curves. In Fig. 1(a), we show the shape space and the data points in it. The shape space is represented with a high-dimensional sphere. In shape space, the data have same scale and same center, which can be expressed in a sphere intuitively. The geodesic path in shape space can be represented by arc length in the high-dimensional sphere. Therefore the shape q_0, q_1 and the geodesic path between them can be represented in a sphere visually.

$$\alpha(\tau) = \frac{1}{\sin(\theta)} (\sin(\theta(1-\tau)) q_0 + \sin(\theta\tau) q_1) \tag{4}$$

$$d(q_0, q_1) = \cos(\langle q_0, q_1 \rangle), \theta = \arccos(\langle q_0, q_1 \rangle) \tag{5}$$

Considering the influence of the curves' presentation, the SRV provides a representation method called the elastic metric to handle such influence. This method can be regarded as a correspondence between two curves with a minimum energy consumption. The SRV provides an elastic metric for the curves in the pre-shape space. Dynamic programming is used to reduce the representations' energy in Eq. (6) between the curves' geodesic length ζ, which can be treated as an alignment. More details are discussed in [38].

$$E(\zeta) = \frac{1}{2} \int_0^1 \left\langle \frac{d\zeta}{d\tau}(\tau), \frac{d\zeta}{d\tau}(\tau) \right\rangle d\tau \tag{6}$$

4. Nose similarity measure

In our method, we construct the nose shape based on a set of nose curves. The similarity measure of the nose shape is computed using the metric of nose curves in the shape space. Firstly, we introduce the nose curves. The curves satisfy certain constraints, such as convenient for registration for different faces and representing the main geometric features of the nose area; the curves are not sensitive to different accuracies of the triangular meshes. Next, we provide the metric of the nose curves in the curves shape space. Combining the metric results on the curves, we can achieve the similarity measure result of the nose shape.

4.1. Nose curves

Comparing a 3D surface similarity measure through certain curves has been investigated in some research studies. Using geodesic circles or curves in certain facial regions to represent the shape is the usual approach ([1,28] and [39]). Usually, the geodesic circles can represent the shape of the facial surface. However, the 3D surface is achieved by scanning instruments, and the surface precision is limited by the triangular meshes of the scanning and pre-processing results on the 3D object. The coarse triangular meshes produce noise in the geodesic circles. We extract a new set of nose curves, which cross the bridge of the nose. The bridge of the nose is the geodesic path between the nasal tip and the center of the eyebrows. The nose curves are chosen from the nose area that has obvious geometric features. The curves represent the shape of the nose in a direct manner. The nose curves are robust to noise induced by the triangular meshes.

The definition of nose curves is a set of geodesic curves that are orthogonal to the bridge of the nose. One end point of the nose curve is in the bridge of the nose, and the other is in the geodesic circle that has a certain geodesic distance (the geodesic distance between nasal tip and the center of eyebrows) to the nasal tip. The nose curves can represent the geometric features of the nose region.

$$N_c = \{G(c, l) | l \in Cb, c \in S, T_l\{G(c, l)\} \perp T_l\{Cb\}\} \tag{7}$$

In Eq. (7), N_c represents the set of nose curves obtained from facial data, which can be regarded as the nose shape . Cb is the bridge of the nose, and l is the point on Cb. $G(c, l)$ is the geodesic

curve in the facial surface with two end points c and l. Additionally, c is the point in the geodesic circle S that has a certain geodesic distance to the nasal tip. The tangent vector $T_l\{G(c, l)\}$ of the geodesic path $G(c, l)$ is perpendicular to the tangent vector $T_l\{Cb\}$ of Cb at point l. By default, the specific geodesic distance is the geodesic distance between the nasal tip and the center of the eyebrows. The surface of the nose region is constructed by the N_c. In Fig. 1(b), we show the instances of several nose curves in the 3D facial surface. P_n is the nasal tip, and P_e is the center of the eyebrows, and $Cb = G(P_e, P_n)$, the distance of Cb, is equal to $G(cn, P_n)$.

4.2. Nose measure in the curves shape space

Using the nose curves, we can define the similarity measure of noses. The nose measure can be regarded as the measure of nose curves in the curves shape space. Essentially, the measure is defined by the geodesic distance between two curves in the shape space. In Eq. (8), we show the nose measure between two noses.

$$d(N_1, N_2) = \int_{Cb} G_s(C_{1l}, C_{2l}) d(l) \tag{8}$$

N_1 and N_2 are two noses, which are represented by nose curves respectively. G_s is the measure between two nose curves in the curves shape space. In the discrete case, the nose measure is shown in Eq. (9). Here, k is the number of nose curves from one nose.

$$d(N_1, N_2) = \sum_{l=1}^{k} G_s(C_{1l}, C_{2l}) \tag{9}$$

To obtain the measurement of Eq. (9), we should compute G_s from two curves. In Section 3, we discussed the background knowledge on the shape space and SRV. Our basic idea for a curves measure in shape space is similar to SRV. We remove the elastic metric and simplify the representation to curves in the shape space. The elastic metric of the nose curves reduces the individual differences between the noses. We propose a simpler representation for a nose curve that preserves the precision of the nose shape and provides a convenient computational method. Firstly, we introduce the curve's representation in shape space. The representation is a discrete form which is shown in Eq. (10).

$$C_v = \{v_1, \ldots, v_h\}, C_v(t) = v_t, v_t \in C_v \tag{10}$$

C_v is the arc length parameterization of the nose curve, and it includes a set of vectors to represent the curve, where v is a vector in C_v, which achieved by two adjacent points in the curve. Here, h is the number of points in the curve. C_v represents the continuity curves when h tends to infinity. In practice, h is a certain constant that changes the continuity problem to a discrete problem. Using the representation of the curves, we achieve the data form in shape space. In Section 3, we discussed that the action group influence should be removed. In Eq. 11, we normalize the vectors in C_v. The vectors in C_v are represented by a direction vector multiplied by a specific step length. The direction vector can be achieved by the original vector's unitization. The specific amount is the reciprocal of k. The representation is invariant to scaling and translation.

$$C_{vs} = \{v_1', \ldots, v_h'\}, v_t' = v_t/(h \cdot \|v_t\|), \sum_{t=1}^{h} \|v_t'\| = 1 \tag{11}$$

In Eq. (11), the direction vector is limited by the coordinate system, and the influence of rotation still exists. To solve the problem, we establish a local coordinate system to transfer the vectors in C_{vs}. The local coordinate system is based on the nasal tip and the eyebrows' center in the 3D facial surface. First, we compute the geodesic path between the nasal tip and the eyebrows' center. Then, the tangent direction of the path at the nasal tip is achieved. The geodesic path computing methods are researched by many years. In our method, we use a classical method [50] to search the geodesic path in facial surface. Next, we use the path to compute another geodesic path that crosses the nasal tip, and the tangent direction is perpendicular to first direction. Finally, we use the two tangent directions to achieve the third direction by a cross-product. We use the three directions to build the local coordinate system. The local coordinate system based on nasal region has been explained in [51]. Although there are subtle differences in specific implementations between different methods, the core idea is the same. The vectors in C_{vs} are transformed to the local coordinate system by T in Eq. (12). Using the new vector representation, we achieve the geodesic distance between the two curves in shape space in Eq. (13).

$$C_{vs}' = \{T(v_1'), \ldots, T(v_h')\} \tag{12}$$

$$G_s(C_1, C_2) = \arccos\left\langle C_{vs1}', C_{vs2}' \right\rangle \tag{13}$$

Combining Eqs. (9) and (13), we achieve the nose similarity measure result. The nose shape is represented and measured by the nose curves. In Eq. (5), the curve in the geodesic path between the two curves is given. We use the equation to illustrate the changes in the nose curves between the two noses. In Fig. 2, we show the instance ($\tau = 0, 0.2, 0.4, 0.6, 0.8, 1$).

Here, G_s is a mathematical metric for the nose curves since it satisfies the following properties. (1) The nose curves measure in the curves shape space can be regarded as included angle of the two vectors. The range of the angle is $[0, \pi]$. If the angle is 0, then the vectors are equal. G_s satisfies the positivity property. (2) The included angle of the two vectors is symmetrical, and G_s satisfies the symmetry property. (3) Suppose that C_1 and C_2 are nose curves in the curves shape space, and C_t is another nose curve in the space. The position of C_t has two different situations, depending on whether C_t is in the geodesic path between C_1 and C_2. The geodesic distance between C_1 and C_2 can be regarded as the included angle in the curves shape space, and it is the smallest distance in the space. If C_t is not in the geodesic path between C_1 and C_2, then $G_s(C_1, C_2) < G_s(C_1, C_t) + G_s(C_t, C_2)$. If C_t is in the geodesic path between C_1 and C_2, then C_t satisfies Eq. (5), $G_s(C_1, C_2) = G_s(C_1, C_t) + G_s(C_t, C_2)$. G_s satisfies the triangle inequality property. The nose similarity measure is a linear combination of the nose curves measure, and thus, the nose measure is also a mathematical metric.

5. Applications and experiments

Using the nose similarity measure, we can construct a nasal hierarchical structure for facial data organization. The nasal hierarchical structure can be utilized in facial classification and facial identification. We illustrate our method's performance in this section. We employ three public 3D facial databases namely, FRGC2.0, Texas3D [52] and BosphorusDB for experimentation. These databases are widely used in facial data analysis. We select facial data from Fall2003 in FRGC2.0 to build the nasal structure (348*3) and other facial data to be the test set. We select 215 facial scans from 113 people in Texas3D (some people just have single scan in the database) to build the nasal structure and other facial data to be the test set. We select 315 samples from 105 persons in BosphorusDB to build the nasal structure and other facial data to be the test set. To illustrate the advantages of our method, we reduce the sampling point's rate for 5%-25% in the surface reconstruction for the three tests (FRGC2.0: 5% - 25%, Texas3D: 5%, BosphorusDB: 25%; Using the full images in our method can achieve more accuracy result, however, the speed of the geodesic path computation is unacceptable).

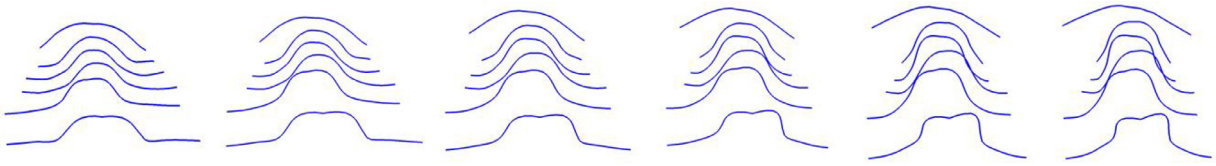

Fig. 2. The nose curves' variations following the geodesic path between two noses in shape space.

The fully automated system based on our method require two processes: 3D face triangular meshing and facial landmarks detection. Generally, the triangular meshes from rough scanning facial data are obtained difficultly. The reason is some facial regions have complex geometric features and topology structure such as eyes and mouth. Reconstruction of such region is affected by different facial expressions. Using the professional software (such as Geomagic Studio and MeshLab) artificially can solve the problem. However, the process cannot be used in an automated system. In our method, the reconstruction region is restricted to the nasal surface. The geometric features from nasal region is robust to facial expression relatively. The triangular meshing in nasal region is simple than other facial regions. The surface reconstruction method [53] is used to obtain the triangular meshes of nasal region which provides an automatic plan. There have several works for 3D facial landmarks detection method ([54–56]). We adopt the method from [56] to detect the nose tip and center of eyebrows. The method detects the landmarks in 3D facial surface directly and does not require the texture information. Based on the triangular meshes and facial landmarks, the nasal curves can be extracted by geodesic automatically. The geodesic extraction is processed by method [50].

Before we apply the method to measure the nose shapes in the databases, some of the parameters should be fixed. The influence of different landmarks' positions is evaluated in the test set of FRGC2.0. In Eq. (9), different nose curves have the same weight in the nose measure process. In fact, the nose curves at different positions of the nose have different influences. For example, the nose curves have less influence on the nose measure when the curves are nearby the center of the eyebrows where these curves appear relatively similar for different noses. Therefore, we should weight the influence of these nose curves. In Eq. (14), we add a weight w_l to each nose curve for the proposed nose curves measure.

$$d(N_1, N_2) = \sum_{l=1}^{k} w_l G_s(C_{1l}, C_{2l}) \tag{14}$$

The parameters to be determined include the weights of the curves, and the number of nose curves. The weights of the curves are determined by the degree of importance of the nose curves. We employ a linear regression method to obtain the set of weights. In Eq. (14), we want to achieve the minimum value of $d(N_1, N_2)$ when the N_1, N_2 come from same person and maximum value of $d(N_1, N_2)$ when N_1, N_2 come from different persons. We set 0 and π to be two target values for two conditions. Using the least squares algorithm [57] to solve the linear regression problem, the weight values can be achieved. We sort the set of weights and divided them into three parts: 0.5, 1 and 2. The reason is that the weights in the nose measure should be limited in a small range to prevent over fitting and the value of weight can't be negative.

In Fig. 3(a), we compare the receiver operating characteristic curves (ROC) of two weighting configurations based on the Texas3D database: one is computed based on the optimized weights configuration, and the other is computed using the same average weight on every nose curve. The ROC curve is the plot of the true positive rate (TPR) versus the corresponding false positive rate (FPR). TPR is defined as the percentage of the occurrences where an authorized user is correctly accepted by the system, while FPR is defined as the percentage of the occurrences where a non-authorized user is falsely accepted by the system. We use the 122 facial data from the Texas3D test set to be the gallery set and 61 facial data from Texas3D test set to be the probe set. The facial data in probe set should have samples from same persons in gallery set. Based on this data set, we have 122 correctly matched samples (clients) and 14,640 (122*120) incorrectly matched samples (impostors). By varying the decision threshold, the ROC can be obtained. Increasing the number of nose curves improves the accuracy of the nose shape. However, the improvement is not obvious when the number of curves is higher than a threshold. Moreover, redundant curves also increase the computational time. In Fig. 3(b), we show the ROC results of different numbers of nose curves for nose recognition in Texas3D. When the number of nose curves is larger than 5, the recognition rate cannot be improved obviously. The positions of nose curves are located by the method which has been discussed in Section 4.1. In nose bridge curve, we select five points $l1 - l5$ which divide the nose bridge path into same length (same as in Fig. 1b). The $c1 - c5$ are selected by the geodesic stripes. We connect ln and cn by geodesic path which is the half nose curve in our method. Another part of nose curve is achieved by the geodesic path between ln and the mirror symmetry point of cn in face object. Based on these results, we obtain a near optimal configuration of the parameters. Using this set of parameters, we evaluate the influence of landmarks' positions with small perturbations in the evaluation using the FRGC2.0 which have same test scale to Texas3D. The ROC results of the original landmark positions and the two sets of landmark positions ($M1$ and $M2$) with small perturbations are shown in Fig. 3c. This result shows the sensitivity of the results with respect to small perturbations.

Based on the parameters, we construct the formal experiments to evaluate the performance of our method. Firstly, we propose a hierarchical structure for different noses by nose shape measure results. Drira [1] illustrated the advantages of such hierarchical structure. The structure is regarded as an efficient organization for different noses and provides additional improvement for nose analysis, such as nose classification and recognition. Next, we show the performance of our nose shape analysis on certain classification problems. As is known, the facial data have a natural classification such as a classification that is based on gender or ethnicity. The nose shapes in certain natural classes should have similar characteristics to a certain extent. We apply the nose shape analysis and the hierarchical structure information to show the characteristics. Finally, we use the nose shape similarity measure to process the nose recognition tasks in a hierarchical structure. Several methods are discussed and compared with our method.

5.1. Nose shape for hierarchical structure construction

Using the results of nasal similarity measure, we establish a hierarchical structure for nose representation. The structure is regarded as an efficient tree organization for different noses. The noses in the same node or have the same father node in the struc-

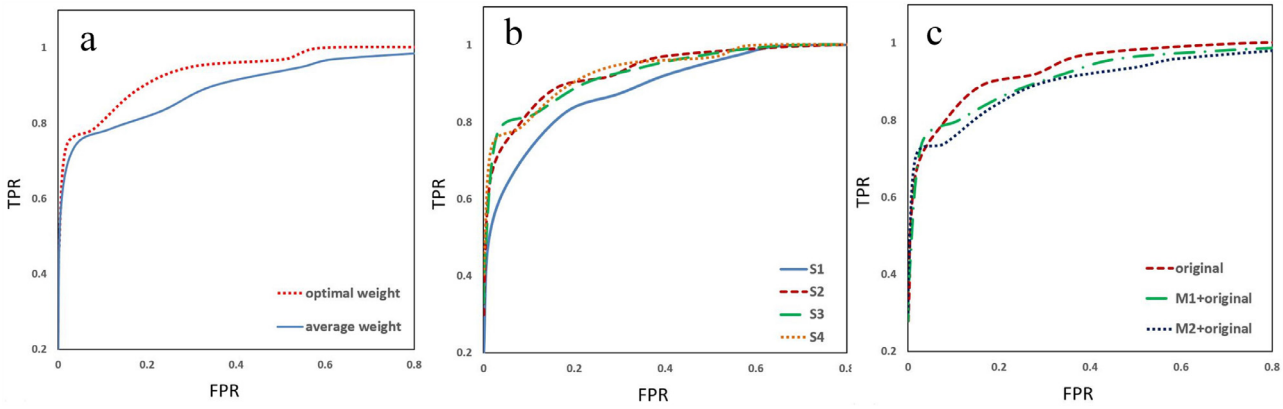

Fig. 3. (a) The ROC plots for two weighting configurations. (b) The ROC result of nose shape analysis with the number of nose curves $S1 = 3, S2 = 5, S3 = 7, S4 = 9$.(c) The ROC result of different landmarks positions arrangement in FRGC2.0. The original positions are detected by [47] and manually correct. M1 and M2 are two arrangements of landmarks positions with small random movements away from the original position.

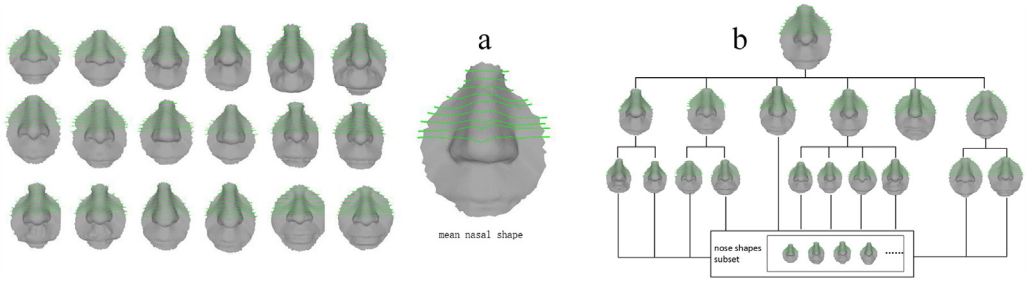

Fig. 4. Nasal data organization. (a) The mean nasal shape of the nose set. (b) The hierarchical structure of nose shapes. The node in the structure can be represented as a mean nose shape. We input the source nose shape in the structure and achieve the nose shape subset.

ture means that their shapes have a close relationship. In a statistical sense, the node in the structure can be represented by a mean nasal shape [1] of the noses in the node. The mean nasal shape is computed using Eqs. (15) and (16).

$$S_N = \{N_1, \ldots N_n\}, V(N_m) = \sum_{i=1}^{n} d(N_m, N_i) \tag{15}$$

$$\overline{N} = \arg\min_{N_m \in S_N} V(N_m) \tag{16}$$

$$E_i = \sum_{j=1}^{r} d(\overline{N}_i, N_{ij}), N_{ij} \in node(i) \tag{17}$$

S_N is the nose set. N is the nose in S_N. $V(N)$ is the sum of distances from N to the other noses in S. $\overline{N}$ is the mean nasal shape of S_N. The mean shape is the center of a nose set (Fig. 4a). It represents the main geometric features of the set. Choosing a suitable classification method can affect the clustering characters of noses. We propose to adopt the energy formula [1] in Eq. (17) for classification. In a node i, the energy is represented by the sum distance from mean shape $\overline{N}_i$ in the node and other nose shape N_{ij} in the node.

Every mean nasal shape $\overline{N}_i$ represents a subset that is a node in the hierarchical structure. The classification energy is the sum of the distances from the mean nasal shape to the nose samples in the subset. The classification scheme with the minimum classification energy is the hierarchical structure. We employ the Affinity Propagation (AP) method [58] to construct the hierarchical structure. For a large database of noses, increasing the number of AP iterations can construct an elaborate hierarchical structure. In Fig. 4b, we show a sample of the hierarchical structure based on the Texas3D database. To evaluate clustering performance in the structure, the analysis of variance (ANOVA) of the facial clustering result from three data sets is shown in Table 1. The value of p is much smaller than 0.05. It shows that the comparison of different facial classes for the clustering is statistically significant.

5.2. Nose shape for facial classification

There are several natural classifications for human faces, such as information regarding gender and ethnicity. Different faces in the same facial class could have similar characters around the nose area, to a certain extent. We establish a simple analysis model to obtain the classification results in FRGC2.0. The simple solution of the model's construct is to compute the mean nasal shapes of the nasal data of different classes. We compare several nose measurement results among the target noses and the mean nasal shapes for facial classification. In practice, we can use a hierarchical structure to construct a framework for gender classification. Firstly, we obtain each of the mean nasal shapes from the nose hierarchical structure. The mean nasal shapes are separated into different gender classes. Next, we compute the similarity between the target nasal data and the mean nasal shapes of each gender class. The closest one is the result of gender classification. The framework can be regarded as a weak classifier.

In Figs. 5(a) and (b), we show the ROC results for classifying human faces by gender and ethnicity from the Texas3D test set. We found that the result of gender classification is not satisfactory. The ROC result for ethnicity classification is better than that for gender classification. The reason is that the nose shapes are sensitive to the different ethnicity of humans. Different nose shapes with different ethnicity affect the accuracy of the gender classification. Although the females' nose shapes are smoother than those of the males in the facial database, at the same time, the nose shapes of Asians are smoother than those of Europeans. We should consider such different conditions of gender and ethnicity combinations. In

Table 1
ANOVA result of tests in FRGC2.0, Texas3D and BosphorusDB.

FRGC2.0						Texas3D					
Source	SS	df	MS	F	p	Source	SS	df	MS	F	p
Groups	34.05	30	1.135	33.44	<<0.05	Groups	14.76	14	1.054	21.54	<<0.05
Error	11.41	336	0.034			Error	4.79	98	0.048		
Total	45.46	336				Total	29.55	112			
BosphorusDB											
Source		**SS**		**df**		**MS**		**F**		**p**	
Groups		7.455		10		0.745		20.4		<<0.05	
Error		3.434		94		0.036					
Total		10.889		104							

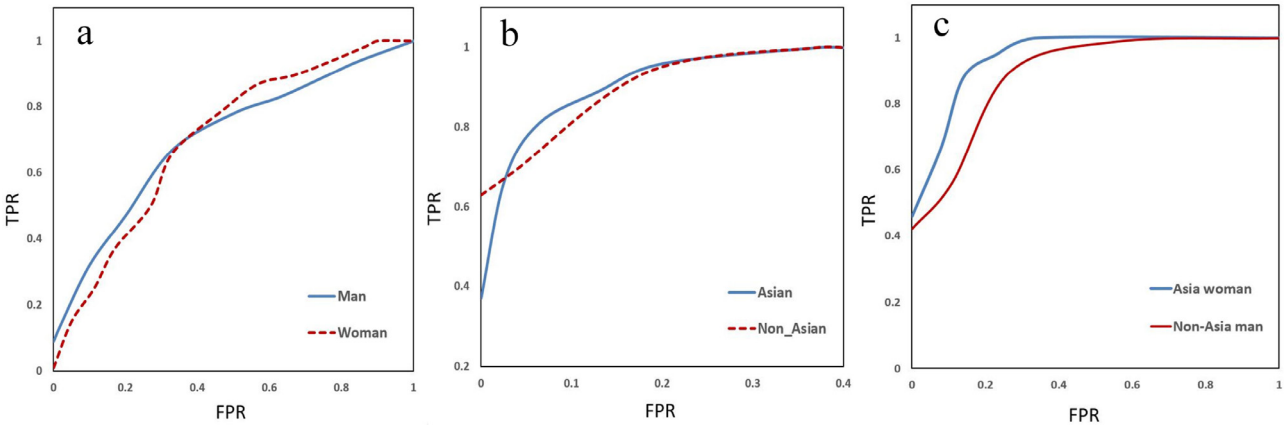

Fig. 5. The ROC results for gender (a) and ethnicity (b) classification by nose shape. (c) The ROC results of certain classifications (Asian women and non-Asian men).

Table 2
The ROC result of gender and ethnicity classification.

Class	FAR0.1	Class	FAR0.1
Gender(male)	0.32	Gender(female)	0.25
Ethnicity(Asian)	0.89	Ethnicity(Non_Asian)	0.91
Asian female	0.88	Non_Asian male	0.61

Table 3
The ROC result of gender and ethnicity classification by two method.

Method	Gender			Ethnicity		
	Female	Male	Overall	Asian	Non-Asian	Overall
[Lu 2006]	81.2%	88.3%	85.6%	89%	95.2%	92.4%
Our method	87.4%	92.3%	89.4%	89.2%	97.4%	93.3%

Fig. 5(c), we show the ROC result of a combined classification. The classification results were significantly improved. In Table 2, we show the ROC result. Using the nose measure, we can achieve a weak gender classifier. Basically, it is consistent with human visual perception.

We input a nose data as source into the hierarchical structure and a nose shape subset can be achieved which is shown in Fig. 4(b). In the subset, the nose shapes have similar shape characters to the source nose data. The similarity property in the subset can be used to construct an accurate classifier. Using a probability distribution function based on the subset, the accurate classification result can be achieved. The functions are shown in Eq. (18) and (19).

$$p_{female}(N_s) = 1 - \left(\frac{\min(d(N_s, N_{female}))}{\min(d(N_s, N_{male})) + \min(d(N_s, N_{female}))} \right) \quad (18)$$

$$p_{Asia}(N_s) = 1 - \left(\frac{\min(d(N_s, N_{Aisa}))}{\min(d(N_s, N_{Asia})) + \min(d(N_s, N_{other}))} \right) \quad (19)$$

The probability function $p(N_s)$ is computed based on the subset which is achieved by the searching result from hierarchical structure. In certain classification problems, we achieve the most similar nose with certain classification characteristics and compute the rate with the most similar nose with other classification characteristics. In Eq. (18), we attempt to achieve the probability of source nose *Ns* belongs to female. Firstly, we compute the distance between nose shapes in subset and source nose data. Next, we achieve the nose shape which belongs to female N_{female} and have minimum distance to source nose data. Then, we achieve the nose shape which belongs to male N_{male} and have minimum distance to source nose data. Finally, we compute the probability of source nose N_s belongs to female based on the two distance values. For ethnicity classification task, the process is similar (Eq. (19). To show the classification performance of our method, we compare our method to competitor [59] in Table 3. The test data come from FRGC2.0 in our test set. The result shows that our method has ability to obtain similar classification rate to professional classification method.

5.3. Nose shape for facial identification

In this section, we evaluate the identification and verification performance based on nose shape analysis methods on three public face databases. The face data in FGRC2.0 have no landmark information. We adopt the landmarks detection method that was discussed in [56]. For most cases, the detection result can be satisfied in our method for nose curves extraction. We just modify the landmarks positions in few face objects during nose curves extraction process. In some situations, we adjust the positions of the landmarks manually due to inaccurate detection. The hierarchical structure of the nose shape is used to improve the efficiency of the calculation. The hierarchical structures are constructed by the

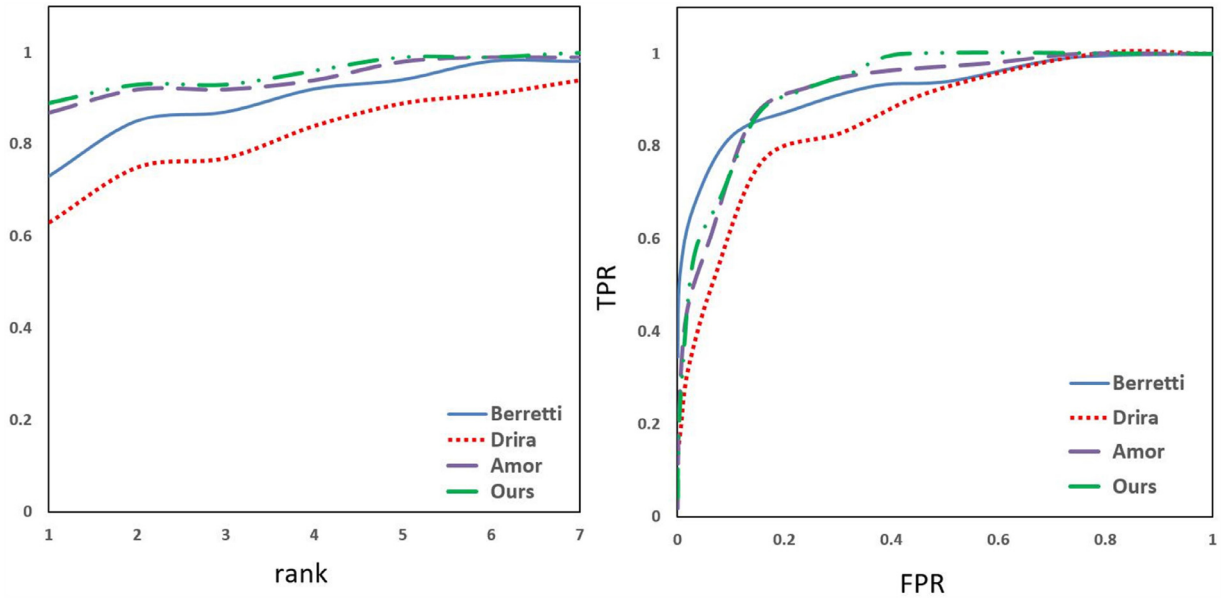

Fig. 6. The CMC and ROC results for identification by different nose analysis methods (FRGC2.0).

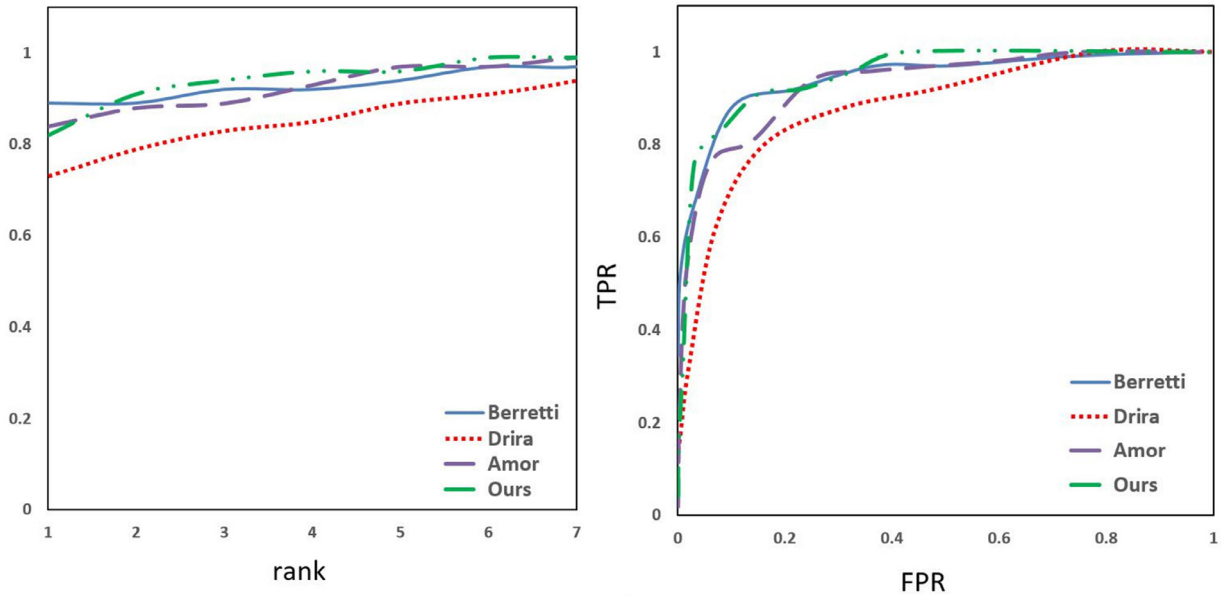

Fig. 7. The CMC and ROC results for identification by different nose analysis methods (Texas3D).

gallery sets. The facial data in probe set should have samples from same person in gallery set.

We consider that the most obvious geometric feature of the nose is the shape near by the nose bridge. The isogeodesic circles [1] and stripes [28] do not follow the bridge of the nose. The nose curves of our method reflects the essential characteristics of the nose shape. To illustrate the advantages of our method, we show the identification rate in the hierarchical structure using different methods. The identification rate reflects the probability that the face data from one person are placed into same node in the hierarchical structure. It is determined by the accuracy of the nasal similarity measure. Using an unreasonable nasal similarity measure cannot obtain an effective hierarchical structure or a high identification rate. Therefore, the identification rate in the hierarchical structure reveals the performance of the similarity measure algorithm. We show the identification results by different methods using Cumulative Matching Characteristics (CMC) and ROC in different facial test sets. The left pictures in Figs. 6–8 are the CMC results. The data in transverse axis represent the rank order in recognition process. The data in longitudinal axis represent the identification rate to corresponding rank value. The right picture in Figs. 6–8 is the ROC result. The data transverse axis represent false positive rate in recognition. The data in longitudinal axis represent true positive rate in recognition. We build the test from three facial databases which have been introduced in first paragraph. In order to show the performance of different methods intuitively, we compute the $L1$ and Hausdorff distance between different CMC curves from Figs. 6–8 in Tables 4 and 5. Basically, the data distributions of two forms are consistent.

In Table 4, the $L1$ distances between CMC curves show the identification performance of different methods. Using our method as a benchmark. For the results based on FRGC 2.0, our method have similar identification rate with Amor [39] and better than other two methods. For Texas3D, the identification rate of Berretti [28] is

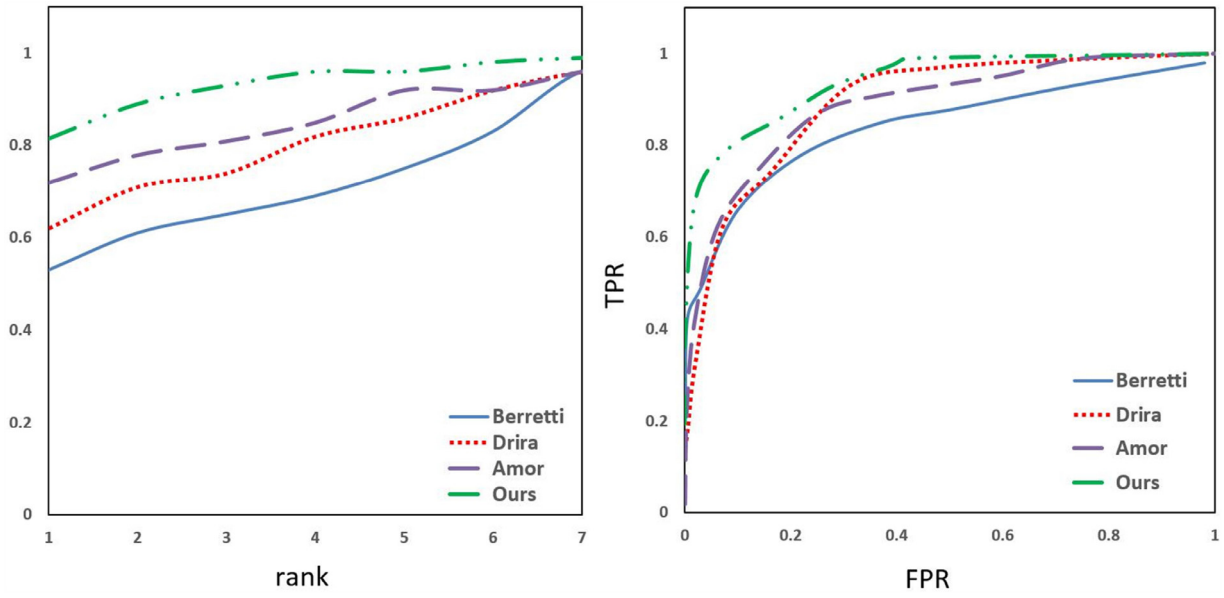

Fig. 8. The CMC and ROC results for identification by different nose analysis methods (BosphorusDB).

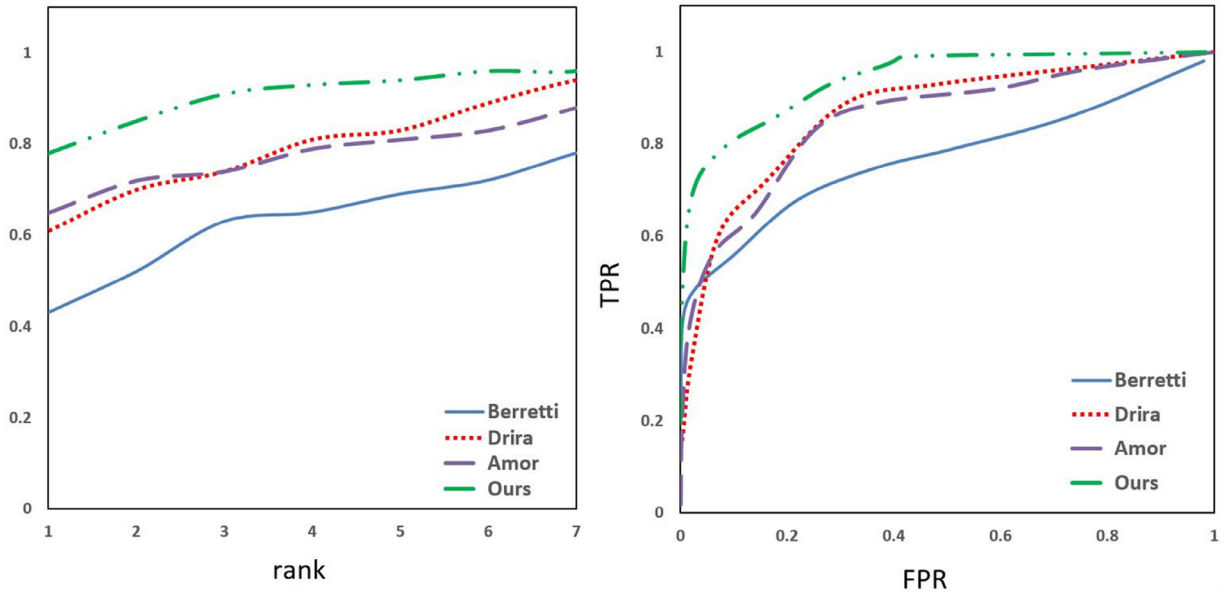

Fig. 9. The CMC and ROC results for identification by different nose analysis methods (sub-test set in BosphorusDB).

Table 4
The $L1$ distance between different curves from CMC results (From Rank1 to Rank7). B: Berretti [28], D: Drira [1], A: Amor [39], O: Our method.

	FRGC2.0				Texas3D				BosphorusDB			
Method	B	D	A	O	B	D	A	O	B	D	A	O
B	0	0.59	0.33	**0.42**	0	0.56	0.22	**0.21**	0	0.65	0.94	**1.51**
D	0.59	0	0.92	**0.99**	0.56	0	0.53	**0.63**	0.65	0	0.33	**0.89**
A	0.33	0.92	0	**0.08**	0.22	0.53	0	**0.16**	0.94	0.33	0	**0.56**
O	0.42	0.99	0.08	**0**	0.21	0.63	0.16	**0**	1.51	0.89	0.56	**0**

Table 5
The Hausdorff distance between different curves from CMC results (From Rank1 to Rank7). B: Berretti [28], D: Drira [1], A: Amor [39], O: Our method.

	FRGC2.0				Texas3D				BosphorusDB			
Method	B	D	A	O	B	D	A	O	B	D	A	O
B	0	0.49	0.24	**0.38**	0	0.46	0.17	**0.17**	0	0.49	0.81	**1.12**
D	0.49	0	0.79	**0.81**	0.46	0	0.43	**0.51**	0.49	0	0.25	**0.72**
A	0.24	0.79	0	**0.05**	0.17	0.43	0	**0.11**	0.81	0.25	0	**0.42**
O	0.38	0.81	0.05	**0**	0.17	0.51	0.11	**0**	1.12	0.72	0.42	**0**

Table 6
The characteristics of different methods. Time_H means the searching time cost with hierarchical structure accelerate. The true rate means the classification rate of the nose shape is classified to correct node in the structure.

Database	FRGC2.0					Texas3D				
Method	Time	Time_H	True Rate	Rank3	FPR0.1	Time	Time_H	True Rate	Rank3	FPR0.1
Berretti 2010	**47s**	–	–	0.87	0.82	**3.6s**	–	–	0.92	0.88
Drira 2009	183s	12.2s	72%	0.77	0.77	22.6s	3.8s	74%	0.83	0.80
Amor 2014	111s	–	–	0.92	0.86	12.52s	–	–	0.89	0.81
Our Method	176s	**11s**	**91%**	**0.93**	**0.87**	14.4s	**2.4s**	**94%**	**0.94**	**0.91**

Database	**BosphorusDB**			
Method	**Time**	**Time_H**	**True Rate**	**Rank3**	**FAR0.1**
Berretti 2010	**3.2s**	–	–	0.65	0.68
Drira 2009	23.5s	4.3s	62%	0.77	0.74
Amor 2014	12.5s	–	–	0.81	0.75
Our Method	18.1s	**3.2s**	**92%**	**0.93**	**0.86**

Table 7
The identification rate of different methods in Rank3.

Method	Facial expressions		Sampling rate		Landmarks with small perturbations	
	neutral	Non-neutral	5%	25%	M1	M2
Berretti 2010	0.87	0.84	0.85	0.88	0.85	0.86
Drira 2009	0.77	0.75	0.72	0.83	0.76	0.74
Amor 2014	0.92	0.88	0.85	0.93	0.90	0.91
Our Method	0.93	0.92	0.92	0.94	0.91	0.92

improved obviously because the method is sensitive to different head poses of facial data and the facial data from Texas3D are aligned. For BosphorusDB, the identification rate of Amor [39] is degenerated obviously because the facial data in BosphorusDB have different kinds of occlusions and facial expressions. The geodesic curves which are selected from Amor [39] are sensitive to such influence factors. The facial data in BosphorusDB also includes different head poses and the identification rate of Berretti [28] also be affected obviously. In Table 6, we show more information about experimental data which includes searching speed (with or without hierarchical structure accelerate) and some identification performance.

The identification rate of different methods in BosphorusDB have significant degradation. It should be noticed that the facial data in BosphorusDB include poses, glasses, hand and hair occlusions. The methods based on the whole face analysis are affected by the conditions obviously. Our method is based on the nasal region, it is robust to such influences. To illustrate the advantages of our method, we build a sub-test in BosphorusDB (105*6), which just includes the facial data with different poses, glass and hair occlusions. The facial data with special poses and hand occlusion can't be generated to the complete triangular meshes. It means such facial data just have half surface can be used. For this conditions, we just extract the nose curves from the half face and build the nose measure, it is based on the symmetry of human face. In Fig. 9, we show the CMC and ROC results in the sub-test set of BosphorusDB.

Based on the experiment results, we also evaluate the identification performance from different classes of facial data using different methods. We select different facial data from the facial databases to build test sets. Firstly, we divide facial data from BosphorusDB and Texas3D into two classes: neutral and Non-neutral. Secondly, we divide facial data from FRGC2.0 into two classes: 5% and 25% sampling rate in trangular meshing process. Thirdly, we divide facial data from FRGC2.0 into two classes with different landmarks' movement: M1 and M2, which have been discussed previously. In Tables 7 and 8, we show the identification rate in Rank3 and TPR data in FAR 0.1 of different methods in corresponding test sets. The result shows that the methods which extract geodesic curves from global facial regions are robust to different facial expressions and landmarks perturbations. However, the methods which use the geodesic curves to be the facial features directly are sensitive to sampling rate. The nose curves of our method solve the problem effectively.

Table 8
The TPR of different methods in FAR0.1.

Method	Facial expressions		Sampling rate		Landmarks with small perturbations	
	neutral	Non-neutral	5%	25%	M1	M2
Berretti 2010	0.82	0.78	0.84	0.87	0.83	0.83
Drira 2009	0.77	0.76	0.75	0.83	0.78	0.77
Amor 2014	0.91	0.86	0.81	0.91	0.89	0.88
Our Method	0.91	0.90	0.91	0.94	0.92	0.91

5.4. Summary of results and discussion

Basically, we evaluate our method by three part: hierarchical structure construction, facial classification and facial identification. For the study of the hierarchical structure of the noses, we have shown that nasal clustering can be effectively obtained where a hierarchical structure can be subsequently constructed. To show the performance of facial classification, we compute the gender and ethnicity classification accuracy based on the hierarchical structure. The classification accuracy is computed using the mean nasal shapes measure of the structure. The ROC result shows that the nasal data with the same node (have same mean nasal shape) has the same gender and ethnicity with high probability. This shows that the nasal hierarchical structure reflects the common features of the facial data to a certain extent. To accurate classification, we propose a probability equation based on the subset in the hierarchical structure. The final result in Table 3 shows that our method can achieve similar classification rate to professional classification method.

To further evaluate our proposal, we show the identification and verification performance based on the CMC and ROC results using different methods ([1,28] and [39]). The methods are using the geodesic curves in recognition process. The identification results have been summarized with different conditions in

Table 4 – 8. The method of Berretti [28] extracts the geodesic stripes from global face to build the facial features. It does not use the geodesic curves to represent the geometric features directly. Therefore it is robust to different sampling rate in different facial objects. However, the method is sensitive to different head poses which limits the performance. The method of Drira [1] extracts the geodesic curves from the nose region directly. Therefore it is robust to different facial expressions and some occlusions in facial surface. However, the geodesic curves which are selected in [1] does not contain the obvious nose shape features, the identification rate of the method is affected by the quality of the facial surface. The method of Amor [39] provides a more accurate method which extracts radius geodesic curves to represent the facial shape information. Using the elastic measure in shape space, the identification rate of the method is robust to different facial expressions. However, the elastic measure between geodesic curves is also affected by the quality of the facial surface. The radius geodesic curves are selected from global facial surface which means the curves are sensitive to different occlusions such as hair, glasses and hand occlusions.

In summary, the experiment results show that our method of nasal measurement can obtain a higher recognition rate than competing state-of-the-arts. The nose curves have regular representation in shape space which contains the obvious shape features from nasal region. The nose curves are robust to head pose, the measure of the curves in shape space is not limited by coordinate system. The nose shape can be represented by the nose curves perfectly. The nasal hierarchical structure by nose shape measure can improve the searching speed of facial recognition. The nose measure is robust to hand, glasses and hair occlusions. It is more convenient to be employed in wild face analysis with complex conditions. In our framework, nose curves are selected by the training process in public facial database. In practical, the users should select the appropriate nose curves for specific facial data, which should provides a balance between accurate and speed.

6. Conclusion

We proposed a representation for nose shape based on the nose curves together with a similarity measure for shape comparison. The nose curves were constructed across the bridge of the nose. These curves reflect the characteristics of the nose shape to the greatest extent. A new simple curve representation convenient for removing the scaling, translation and rotation was constructed. Using this representation, we formulated a curve metric in the shape space where the nose shape similarity can be computed. A hierarchical structure of the nose was also constructed based on the measurement results. Such hierarchical structure can be regarded as an effective organization of the facial data. The advantages of our proposed method include tolerance to noise in surface triangulation and consistency with respect to human perception. We experimentally showed the effectiveness of the proposed method for certain classification and identification tasks. However, it is noted that the nose shape analysis cannot replace the full facial analysis completely. The nose shape represents only partial biometric information.

In future work, we will extract more curves from different facial regions to construct a global facial representation. Using the surface template to match the rough face scan data and the reconstruction facial surface can be used to support the global curves' extraction.

Competing interests

The authors declare that they have no competing interests.

Acknowledgments

This research was partially supported by the National Key Cooperation between the BRICS of China (No. 2017YE0100500), National Key R&D Program of China (No. 2017YFB1002600, No. 2017YFB1402105) and Beijing Natural Science Foundation, China (No. 4172033). We thank the face database Texas3D, FRGCv2.0 and BosphorusDB£©and method's code provider in github. We thank the device support from NVIDIA.

Supplementary material

Supplementary material associated with this article can be found, in the online version, at doi:10.1016/j.patcog.2018.12.006.

References

[1] H. Drira, B.B. Amor, A. Srivastava, M. Daoudi, A Riemannian analysis of 3d nose shapes for partial human biometrics, in: IEEE International Conference on Computer Vision, 2009, pp. 2050–2057.
[2] M. Emambakhsh, A. Evans, Nasal patches and curves for expression-robust 3d face recognition, IEEE Trans. Pattern Anal. Mach. Intell. 39 (5) (2016) 995–1007.
[3] G. Antonini, V. Popovici, J.P. Thiran, Independent component analysis and support vector machine for face feature extraction, in: International Conference on Audio and Video-based Biometric Person Authentication, 2003, pp. 111–118.
[4] M. Sharif, S. Mohsin, R.A. Hanan, M.Y. Javed, M. Raza, Using nose heuristics for efficient face recognition, Sindh Univ. Res. J. 43 (43) (2011) 63–68.
[5] C. Tredoux, A direct measure of facial similarity and its relation to human similarity perceptions, J. Exp. Psychol. Appl. 8 (3) (2002) 180–193.
[6] S. Chopra, R. Hadsell, Y. Lecun, Learning a similarity metric discriminatively, with application to face verification, in: Computer Vision and Pattern Recognition, 2005, pp. 539–546.
[7] F. Schroff, T. Treibitz, D. Kriegman, S. Belongie, Pose, illumination and expression invariant pairwise face-similarity measure via doppelgänger list comparison, in: IEEE International Conference on Computer Vision, 2013, pp. 2494–2501.
[8] E. Mostafa, A. Farag, A. Shalaby, A. Ali, T. Gault, A. Mahmoud, Long term facial parts tracking in thermal imaging for uncooperative emotion recognition, in: IEEE Sixth International Conference on Biometrics: Theory, Applications and Systems, 2014, pp. 1–6.
[9] E. Mostafa, A.A. Ali, A. Shalaby, A. Farag, A facial features detector integrating holistic facial information and part-based model, in: Computer Vision and Pattern Recognition Workshops, 2015, pp. 93–99.
[10] A.E. Barkouky, A. Shalaby, A. Mahmoud, A. Farag, Selective part models for detecting partially occluded faces in the wild, in: IEEE International Conference on Image Processing, 2015, pp. 268–272.
[11] J. Soldera, K. Dodson, J. Scharcanski, Face recognition based on geodesic distance approximations between multivariate normal distributions, in: IEEE International Conference on Imaging Systems and Techniques, 2017, pp. 1–6.
[12] Y. Wang, G. Pan, Z. Wu, Y. Wang, Exploring facial expression effects in 3d face recognition using partial icp, in: Asian Conference on Computer Vision, 2006, pp. 581–590.
[13] K.J. Chang, K.W. Bowyer, P.J. Flynn, Effects on facial expression in 3d face recognition, in: SPIE Conf. Biometric Technology for Human Identification, 2005, pp. 132–143.
[14] B. Gokberk, A.A. Salah, L. Akarun, Rank-based decision fusion for 3d shape-based face recognition, in: IEEE Signal Processing and Communications Applications Conference, 2005, pp. 364–367.
[15] A.S. Mian, M. Bennamoun, R. Owens, An efficient multimodal 2d-3d hybrid approach to automatic face recognition, IEEE Trans. Pattern Anal. Mach Intell. 29 (11) (2007) 1927–1943.
[16] C.C. Queirolo, L. Silva, O.R.P. Bellon, M.P. Segundo, 3D face recognition using simulated annealing and the surface interpenetration measure, IEEE Trans. Pattern Anal. Mach. Intell. 32 (2) (2010) 206–219.
[17] D. Li, W. Pedrycz, A central profile-based 3d face pose estimation, Pattern Recognit. 47 (2) (2014) 525–534.
[18] B. Efraty, E. Bilgazyev, S. Shah, I.A. Kakadiaris, Profile-based 3d-aided face recognition, Pattern Recognit. 45 (1) (2012) 43–53.
[19] Y. Lei, M. Bennamoun, M. Hayat, Y. Guo, An efficient 3d face recognition approach using local geometrical signatures, Pattern Recognit. 47 (2) (2014) 509–524.
[20] V. Blanz, T. Vetter, A morphable model for the synthesis of 3d faces, in: SIGGRAPH, 1999, pp. 187–194.
[21] V. Blanz, T. Vetter, Face recognition based on fitting a 3d morphable model, IEEE Trans. Pattern Anal. Mach. Intell. 25 (9) (2003) 1063–1074.
[22] M.W. Lee, S. Ranganath, Pose-invariant face recognition using a 3d deformable model, Pattern Recognit. 36 (8) (2003) 1835–1846.
[23] I.A. Kakadiaris, G. Passalis, G. Toderici, M.N. Murtuza, Y. Lu, N. Karampatziakis, T. Theoharis, Three-dimensional face recognition in the presence of facial expressions: an annotated deformable model approach, IEEE Trans. Pattern Anal. Mach. Intell. 29 (4) (2007) 640–649.

[24] I.A. Kakadiaris, G. Toderici, G. Evangelopoulos, G. Passalis, D. Chu, X. Zhao, S.K. Shah, T. Theoharis, 3D-2D face recognition with pose and illumination normalization, Comput. Vision Image Understanding 154 (2017) 137–151.
[25] G. Hu, F. Yan, J. Kittler, W. Christmas, C.H. Chan, Z. Feng, P. Huber, Efficient 3d morphable face model fitting, Pattern Recognit. 67 (2017) 366–379.
[26] W. Hariri, H. Tabia, N. Farah, A. Benouareth, D. Declercq, 3D face recognition using covariance based descriptors, Pattern Recognit. Lett. 78 (2016) 1–7.
[27] Y. Guo, Y. Lei, L. Liu, Y. Wang, M. Bennamoun, F. Sohel, Ei3d: expression-invariant 3d face recognition based on feature and shape matching, Pattern Recognit. Lett. 83 (2016) 403–412.
[28] S. Berretti, B.A. Del, P. Pala, 3D face recognition using isogeodesic stripes, IEEE Trans. Pattern Anal. Mach. Intell. 32 (12) (2010) 2162–2177.
[29] S. Berretti, A.D. Bimbo, P. Pala, Distinguishing facial features for ethnicity-based 3d face recognition, ACM Trans. Intell. Syst. Technol. 3 (3) (2012) 1–20.
[30] R. Ahdid, E.M. Barrah, S. Safi, B. Manaut, Facial surface analysis using isogeodesic curves in three dimensional face recognition system (2016). arXiv: 1608.08878v1[cs.CV]. 1–6.
[31] A.M. Bronstein, M.M. Bronstein, R. Kimmel, Expression-invariant representations of faces, IEEE Trans. Image Process. 16 (1) (2007) 188–197.
[32] A.M. Bronstein, M.M. Bronstein, R. Kimmel, Three-dimensional face recognition, Int. J. Comput. Vis. 64 (1) (2005) 5–30.
[33] J. Xia, Y. He, D.P.T. Quynh, X. Chen, S.C.H. Hoi, Modeling 3d facial expressions using geometry videos, in: International Conference on Multimedea, 2010, pp. 591–600.
[34] J. Xia, D.T.P. Quynh, Y. He, X. Chen, S.C.H. Hoi, Modeling and compressing 3-d facial expressions using geometry videos, IEEE Trans. Circuits Syst. Video Technol. 22 (1) (2012) 77–90.
[35] W. Zeng, D. Samaras, D.X. Gu, Ricci flow for 3d shape analysis, IEEE Trans. Pattern Anal. Mach. Intell. 32 (4) (2010) 662–677.
[36] W. Zeng, D.X. Gu, Conformal geometric methods in computer vision, in: International Conference and Expo on Emerging Technologies for A Smarter World, 2011, pp. 1–6.
[37] D.G. Kendall, Shape manifolds, procrustean metrics, and complex projective spaces, Bull. London Math. Soc. 16 (2) (1984) 81–121.
[38] A. Srivastava, E. Klassen, S.H. Joshi, I.H. Jermyn, Shape analysis of elastic curves in euclidean spaces, IEEE Trans. Pattern. Anal. Mach. Intell. 33 (7) (2011) 1415–1428.
[39] B.B. Amor, H. Drira, S. Berretti, M. Daoudi, A. Srivastava, 4-D facial expression recognition by learning geometric deformations, IEEE Trans. Cybern. 44 (12) (2014) 2443–2457.
[40] I.H. Jermyn, S. Kurtek, E. Klassen, A. Srivastava, Elastic shape matching of parameterized surfaces using square root normal fields, in: European Conference on Computer Vision, 2012, pp. 804–817.
[41] S. Kurtek, H. Drira, A comprehensive statistical framework for elastic shape analysis of 3d faces, Comput. Graph. 51 (2015) 52–59.
[42] P. Yan, K.W. Bowyer, Biometric recognition using 3d ear shape, IEEE Trans. Pattern Anal. Mach. Intell. 29 (8) (2007) 1297–1308.
[43] H. Chen, B. Bhanu, Human ear recognition in 3d, IEEE Trans. Pattern Anal. Mach Intell 29 (4) (2007) 718–737.
[44] T.C. Faltemier, K.W. Bowyer, P.J. Flynn, A region ensemble for 3-d face recognition, IEEE Trans. Inf. Forensics Secur. 3 (1) (2008) 62–73.
[45] K.I. Chang, K.W. Bowyer, P.J. Flynn, Multiple nose region matching for 3d face recognition under varying facial expression, IEEE Trans. Pattern Anal. Mach. Intell. 28 (10) (2006) 1695–1700.
[46] M. Emambakhsh, A.N. Evans, M. Smith, Using nasal curves matching for expression robust 3d nose recognition, in: IEEE Sixth International Conference on Biometrics: Theory, Applications and Systems, 2013, pp. 1–8.
[47] J. Gao, A.N. Evans, Expression robust 3d face recognition by matching multi–component local shape descriptors on the nasal and adjoining cheek regions, in: IEEE International Conference and Workshops on Automatic Face and Gesture Recognition, 2015, pp. 1–8.
[48] J. Gao, A. Evans, Using 3d representations of the nasal region for improved landmarking and expression robust recognition, in: Uk Computer Vision Student Workshop, 2015, pp. 4.1–4.11.
[49] N. Zehngut, F. Juefei-Xu, R. Bardia, D.K. Pal, C. Bhagavatula, M. Savvides, Investigating the feasibility of image-based nose biometrics, in: IEEE International Conference on Image Processing, 2015, pp. 522–526.
[50] V. Surazhsky, T. Surazhsky, D. Kirsanov, S.J. Gortler, H. Hoppe, Fast exact and approximate geodesics on meshes, in: SIGGRAPH, 2005, pp. 553–560.
[51] F. Tsalakanidou, F. Forster, S. Malassiotis, M.G. Strintzis, Real-time acquisition of depth and color images using structured light and its application to 3d face recognition, Real-Time Imaging 11 (5) (2005) 358–369.
[52] P.J. Phillips, P.J. Flynn, T. Scruggs, K.W. Bowyer, J. Chang, K. Hoffman, J. Marques, J. Min, W. Worek, Overview of the face recognition grand challenge, in: IEEE Computer Society Conference on Computer Vision and Pattern Recognition, 2005, pp. 947–954.
[53] F. Bernardini, J. Mittleman, H. Rushmeier, C. Silva, The ball-pivoting algorithm for surface reconstruction, IEEE Trans. Vis. Comput. Graph. 5 (4) (1999) 349–359.
[54] M.P. Segundo, L. Silva, O.R.P. Bellon, C.C. Queirolo, Automatic face segmentation and facial landmark detection in range images, IEEE Trans. Syst. Man Cybern. 40 (5) (2010) 1319.
[55] Y. Wang, J. Liu, X. Tang, Robust 3d face recognition by local shape difference boosting, IEEE Trans. Pattern Anal. Mach. Intell. 32 (10) (2010) 1858–1870.
[56] F.M. Sukno, J.L. Waddington, P.F. Whelan, 3-D facial landmark localization with asymmetry patterns and shape regression from incomplete local features, IEEE Trans. Cybern. 45 (9) (2017) 1717–1730.
[57] M. Suliman, T. Ballal, A. Kammoun, T.Y. Al-Naffouri, Penalized linear regression for discrete ill-posed problems: A hybrid least-squares and mean-squared error approach, in: Signal Processing Conference, 2016.
[58] B.J. Frey, D. Dueck, Clustering by passing messages between data points, Science 315 (5814) (2007) 972–976.
[59] X. Lu, H. Chen, A.K. Jain, Multimodal facial gender and ethnicity identification, in: International Conference on Biometrics, 2006, pp. 554–561.

Chenlei Lv is studying for PhD degree in College of information science and technology, Beijing Normal University (BNU). His research interests include computer vision, 3D biometrics, computer graphic, discrete differential geometry and conformal geometric.

Zhongke Wu is Full Professor in College of information science and technology, Beijing Normal University (BNU), China. Currently he is the member of Steering Committee for Professional Teaching of Animation, digital media in Colleges and universities of Ministry of Education, China and member of CCF CAD and Graphics and CCF Human Computer Interaction. He led and took part in various research and development projects in computer graphics and related areas. His current research interests include computer graphics, animation virtual reality, geometric modeling, volume graphics and medical imaging.

Xingce Wang is Full Professor in College of Information Science and Technology, Beijing Normal University, PR China. She is major in the 3D modeling and 3D visualization. Her current research interests include computer graphic, medical imaging, artificial intelligence and Machine learning.

Mingquan Zhou is the super visor of doctor candidates and the dean in College of Information Science and Technology, Beijing Normal University, PR China. His current research interests include computer graphics, and 3Dvisualization.

Kar-Ann Toh (SM?03) is currently a faculty member of the School of Electrical and Electronic Engineering, Yonsei University, Seoul, Korea. He has made several PCT filings related to biometric applications and has actively published his works. His research interests include biometrics, pattern classification, optimization, and neural networks. Dr. Toh has served as a member of the Technical Program Committee for international conferences related to biometrics and artificial intelligence. He has also served as a Reviewer for international journals including several IEEE Transactions.